INDEX COPERNICUS INTERNATIONAL

Bio-Algorithms and Med-Systems

WWW.BAMSJOURNAL.COM ISSN: 1896-530X

ORIGINAL ARTICLE

Received: 11.12.2023
Accepted: 28.12.2023
Published: 31.12.2023

CITE THIS ARTICLE AS:
Ardebili FT, Niedzwiecki S, Moskal P, on behalf of the J-PET collaboration, "Evaluation of Modular J-PET sensitivity," Bio-Algorithms and Med-Systems vol. 1, no. 1, pp. 132-138, 2023, DOI: 10.5604/01.3001.0054.1973

AUTHORS' CONTRIBUTION:
A – Study Design
B – Data Collection
C – Statistical Analysis
D – Data Interpretation
E – Manuscript Preparation
F – Literature Search
G – Funds Collection

CORRESPONDING AUTHOR:
Faranak Tayefi Ardebili; Marian Smoluchowski Institute of Physics, Faculty of Physics, Astronomy and Applied Computer Science, Jagiellonian University, Krakow, Poland; 11 Łojasiewicza St., 30-348 Kraków, Poland; Phone: +48 510399372; E-mail: faranaktayefi.tayefi.ardebili@doctoral.uj.edu.pl

Evaluation of Modular J-PET sensitivity

Faranak Tayefi Ardebili[1,2,3ABCDEFG] (ORCID: 0000-0003-1490-1291), Szymon Niedźwiecki[1,2,3ABCDEFG] (ORCID: 0000-0002-5953-9479), Paweł Moskal[1,2,3AEFG] (ORCID: 0000-0001-5644-5963), on behalf of the J-PET collaboration

[1]Marian Smoluchowski Institute of Physics, Faculty of Physics, Astronomy and Applied Computer Science, Jagiellonian University, Krakow, Poland
[2]Total-Body Jagiellonian-PET Laboratory, Jagiellonian University, Krakow, Poland
[3]Center for Theranostics, Jagiellonian University, Krakow, Poland

ABSTRACT

The Modular J-PET represents the latest advancement in the Jagiellonian-PET series, utilizing extended plastic scintillator strips. This prototype's modular design enables cost-effective imaging of multi-photon annihilation and positronium, allowing for easy assembly, portability, and versatility. Additionally, its lightweight construction facilitates static bed examinations with a mobile detection system that can be positioned conveniently alongside the patient, negating the requirement for spacious clinical settings. Comprising 24 modules arranged in regular 24-sided polygons circumscribing a 73.9 cm diameter circle, each module integrates 13 scintillator strips, measuring 50 cm in length and 6 *mm* × 24 *mm* in cross-section. Scintillation light is captured at both ends through analog Silicon Photomultipliers (SiPMs). This research presents Sensitivity of the Modular J-PET tomograph, adhering to the NEMA_NU 2-2018 standards. Sensitivity measurement was performed with ^{68}Ge line source inside the 5 sleeves aluminium phantom placed at center of the detector`s field-of-view (FOV) and 10 cm offset from the center of detector. Analyzing the gathered data involved employing the specialized J-PET Framework software, developed within the C++ architecture. To validate the experimental findings, comparisons were made with GATE simulations, wherein the source and phantom were emulated in the same configuration as employed in the actual experiment. The system sensitivity of the Modular J-PET was assessed to be 1.03 ± 0.02 cps/kBq in the center of the detector`s FOV with the peak sensitivity of 2.1 cps/kBq. However, the simulations indicate that at the center of the detector's FOV, the Modular J-PET achieves a system sensitivity of 1.32 ± 0.03 cps/kBq, with a peak sensitivity of 2.9 cps/kBq.

KEYWORDS

Positron emission tomography, plastic scintillator, sensitivity, NEMA standards, GATE, J-PET, medical imaging, total-body PET

INTRODUCTION

Positron Emission Tomography (PET) is the most advanced molecular imaging method for assessing disease activity at the molecular and cellular levels [1]. The concept of PET dates back to the 1950s, and the first tomographs with clinical uses were produced in the 1970s. Since then, many technological advancements have enabled a constant search for improved systems [2–4]. The J-PET Collaboration has developed a novel prototype PET system at Jagiellonian University in Krakow, Poland, which is cost-effective and enables multi-photon and positronium imaging [5–11]. Its innovation arises from applying plastic scintillators instead of inorganic crystals used in classical PET scanners [7, 12, 13].

J-PET scanner may constitute an economical alternative for crystal PET scanners since plastic scintillators are more than an order of magnitude cheaper than crystals. In addition, the utilization of plastic PET with axially arranged scintillator strips decreases significantly costs of readout electronics and SiPMs for the J-PET scanner, which are expected to be about five times less than the current crystal--based PET tomograph [14]. However, the efficiency of plastic scintillators is rather low. The linear attenuation coefficient for the 511 keV photons for the plastic scintillator is much lower than the crystal scintillator (0.096 1/cm for plastic scintillator with respect to 0. 83 1/cm for LYSO) [15]. This implies that in a single scintillator layer with a typical thickness of PET scan (2–3 cm) [2], in the case of crystal scintillator, most of the annihilation photons hitting the detector are detected, but in the case of plastic scintillators only about a quarter (17–25%) of annihilation photons are detected with the detector [2, 6, 15]. Although plastic scintillators exhibit a lower efficiency compared to crystals, this limitation can potentially be mitigated through the utilization of a multi-layer geometry approach employing axially arranged strips [6]. The significantly lower light attenuation in plastic with respect to crystals enables the effective light transport in long strips [16–18]. Another disadvantage of plastic scintillators is the negligible fraction of the photo-electric effect for the interaction of 511 keV photons. However, it does not preclude the possibility of the scatter fraction reduction; because in the plastic scintillators, the detection of 511 keV gamma quanta is based in practice only on the Compton scattering, and the by setting the threshold on energy deposition on 200 keV [7] a scatter fraction can be reduced below 40% [18].

The Modular J-PET scanner employed in this study is the latest generation of J-PET scanners developed by J-PET collaboration, as depicted in Fig. 1. Modular J-PET utilizes unique detection principles thanks to its novel detector arrangements [10–14]. Application of the triggerless data acquisition system [19], enables the execution of multi-photon and positronium imaging. The construction of Modular J-PET from plastic scintillator, alongside its unique detection principles, facilitates the acquisition of 50 cm of the AFOV [20–24]. The National Electrical Manufacturers Association (NEMA), the association of medical imaging and electrical equipment manufacturers in the United States, publishes

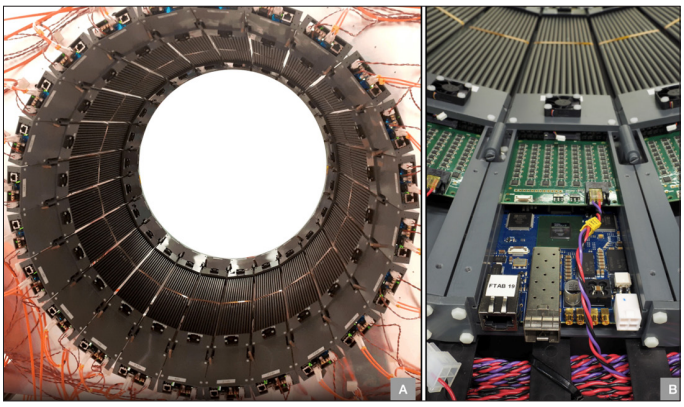

Fig. 1. (A) Illustrates the Modular J-PET detector, comprising 24 modules. Each module consists of 13 scintillator strips, with readout facilitated by a 1 × 4 SiPM array on both ends. These modules allow convenient removal for maintenance purposes, with a total weight of approximately 2 kg. Analog signals undergo digitization in close proximity to the SiPMs via specialized TDC boards developed by the J-PET group; (B) Depicts the power supply board (green), responsible for supplying voltage individually to each SiPM. Additionally, the TDC board (blue) performs the conversion of analog signals to digital format, retaining information regarding signal crossings at two preselected constant thresholds [22].

medical diagnostic imaging equipment standards. One of its standards is NEMA-NU-2, which pertains to PET scanners [25]. The objective of this article is to assess the sensitivity of the Modular J-PET scanner in alignment with the NEMA-NU2_2018 standards. The empirical findings obtained were cross-validated using Monte Carlo simulations facilitated by GATE software. Future work will present all characteristics of Modular J-PET based on the experimental data and simulation.

METHOD AND MATERIALS

Design of the Modular J-PET

The Modular J-PET scanner comprises 24 detection modules, each composed of 13 BC-404 rectangular plastic scintillator strips measuring 24 mm x 6 mm x 500 mm. These strips are arranged axially, forming a symmetrical 24-sided polygon that encloses the scanner. This configuration provides an AFOV spanning a total of 50 cm, with a scanner diameter measuring 73.9 cm as depicted in Fig. 1. [21, 23]. In order to enhance the propagation of light and ensure impermeability to light leakage, plastic scintillator strips are enveloped using a combination of Vikuiti Enhanced Specular Reflector (ESR) foil and DuPont Kapton 100B film [26–28]. Each plastic scintillator is read out on both ends by 4 Hamamatsu-S13 Silicon Photomultipliers (SiPMs) with an area of 6 x 6 mm^2. When a gamma quanta interacts within a scintillator strip, four timestamps are generated – two at the leading edge and two at the trailing edge – across the eight SiPMs. These timestamps, captured by the front-end electronics, are continuously collected by the Data Acquisition System (DAQ). The functionality of the J-PET DAQ System is rooted in its Field-Programmable Gate Array

(FPGA) electronics, enabling the efficient real-time processing of multiple data streams through pipelined operations [29].

Determination of the Modular J-PET sensitivity

The sensitivity of a PET scanner is defined as the number of counts per unit of time detected by the detector for each unit of activity present in a source [25]. The sensitivity of a PET scanner is expressed as a true coincidence events rate (cps/kBq). Sensitivity assessments were performed utilizing a 70 cm sensitivity phantom, located at the centre of detectors FOV and a 10 cm offset from the center of detector's FOV. The sensitivity phantom is composed of 5 aluminium sleeves, with the 2.5 mm thickness and different diameters (as listed in Tab. I.), to minimize the effect of attenuation. The sensitivity measurements were carried out utilizing a 70 cm ^{68}Ge line source with an activity level of 2.6 MBq for 6 hours. Separate measurements were performed through adding one layer of aluminium at each step. The choice of a 6-hour duration alongside of 2.6 MBq activity of the line source meet NEMA_NU2--2018 standards criterion, which recommend collecting data for a period ensuring the acquisition of at least 10,000 trues per slice. The total system sensitivity represents its capability to detect gamma photons emitted from positron annihilation events within the patient's body and was conducted using the following formula:

$$S_{total} = \frac{R_0}{A_{norm}} \quad \text{(eq. 1)}$$

where, R_0 stand for the unattenuated count rate and, A_{norm} stand for normalized activity. To account for uncertainties, the error propagation principle was applied in the determination of

$$\delta(S_{total}) = \frac{\delta(R_0)}{A_{norm}} . \quad \text{(eq. 2)}$$

Normalization of the source's activity within the detector was necessary due to differing lengths of the AFOV detector and the line source, determined as follows:

$$A_{norm} = A_{cal} \times \frac{50cm}{70cm} . \quad \text{(eq. 3)}$$

where, A_{cal} denotes the corrected initial activity. Subsequent analysis relied on normalized activity value of 1.8 MBq. The axial sensitivity profile is derived by plotting the sensitivity for individual slices, utilizing measurements obtained with the smallest tube (R1) placed at the centre of the detectors FOV.

Event selection criteria

The collected data underwent analysis using a dedicated C++ language-based framework [12, 30]. Within the dataset, interactions resulting from a single positron-electron annihilation and all subsequent interactions of secondary particles formed a sequence of consecutive photon interactions, constituting a single event. Coincidence events arose from any two scatterings within an event, provided their interaction times fell within a 4 ns time window. Detected coincidence events were categorized into three types: true coincidences, scatter coincidences, and accidental (or random) coincidences [13]. Fig. 2. present different type of coincidence event, that in both scatter and accidental coincidence events, the annihilation event didn't align with the apparent line of response between the two-photon detections. Such scattered and random coincidences contributed to background noise, thereby diminishing image quality. To reduce background coincidence events, the initial data selection phase involved removing all events with one, three, or more hits, while retaining only those events that exhibited precisely two hits within the 4 ns coincidence time window.

Tab. I. Sensitivity measurement phantom details.

TUBE NUMBER	INSIDE DIAMETER (mm)	OUTSIDE DIAMETER (mm)	LENGTH L (mm)
1	3.9	6.4	700
2	7.0	9.5	700
3	10.2	12.7	700
4	13.4	15.9	700
5	16.6	19.1	700

The number of SiPMs connected to a single scintillator which give the signal was defined as multiplicity cut. A multiplicity cut equal to 8 SiPM signals is expected in the ideal case. Multiplicity cut was the subsequent stage of the data selection.

Further data refinement involved assessing the hit distribution origin based on the estimated energy deposition in a scintillator strip, derived from the time-over-threshold (TOT) values using the relation established in reference [31]. Fig. 3. illustrates the histogram of the sum of TOT values from two thresholds (30 mV and 70 mV) from both sides of each scintillator in the Modular J-PET prototype. Subsequently, a TOT range spanning from 2824 ns.mV to 4801 ns.mV was applied for future analyses. Moreover, limitations were imposed on the FOV of the Modular J-PET in the x and y directions, confined within a circle with a radius of 30 cm. Additionally, the z-coordinate of the annihilation position was restricted within a range of ± 25 cm, rejecting all events with larger z-coordinate values.

The residual background was suppressed using the scatter test (ST) criterion. For hits assigned to annihilation photons (t_i, r_i) and (t_j, r_j), the ST was defined as the difference between the measured times ($\Delta t = |t_j - t_i|$) and the time the photon would require to travel from r_j to r_i ($ST = \delta_{i,j} = d_{i,j} - c \cdot |\Delta t_{i,j}|$, where $d_{i,j}$ is the distance between the i-th and j-th recorded interactions, and $\Delta t_{i,j}$ is the difference in

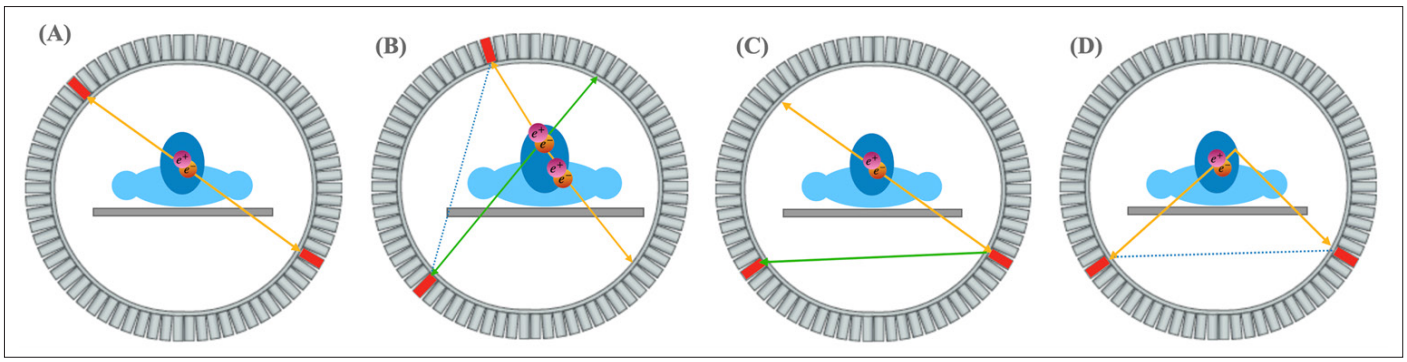

Fig. 2. (A) Illustrates the schematic definitions of different types of coincidences: (a) true coincidence; (B) random coincidence; (C) detector-scattered coincidence, and (D) phantom-scattered coincidence. Central circle represents the patient, while the red detectors signify specific interactions of gamma quanta within the detectors. In background coincidence events, the annihilation event (indicated with e+,e-) doesn't correspond to the anticipated line of response between the two detected photons.

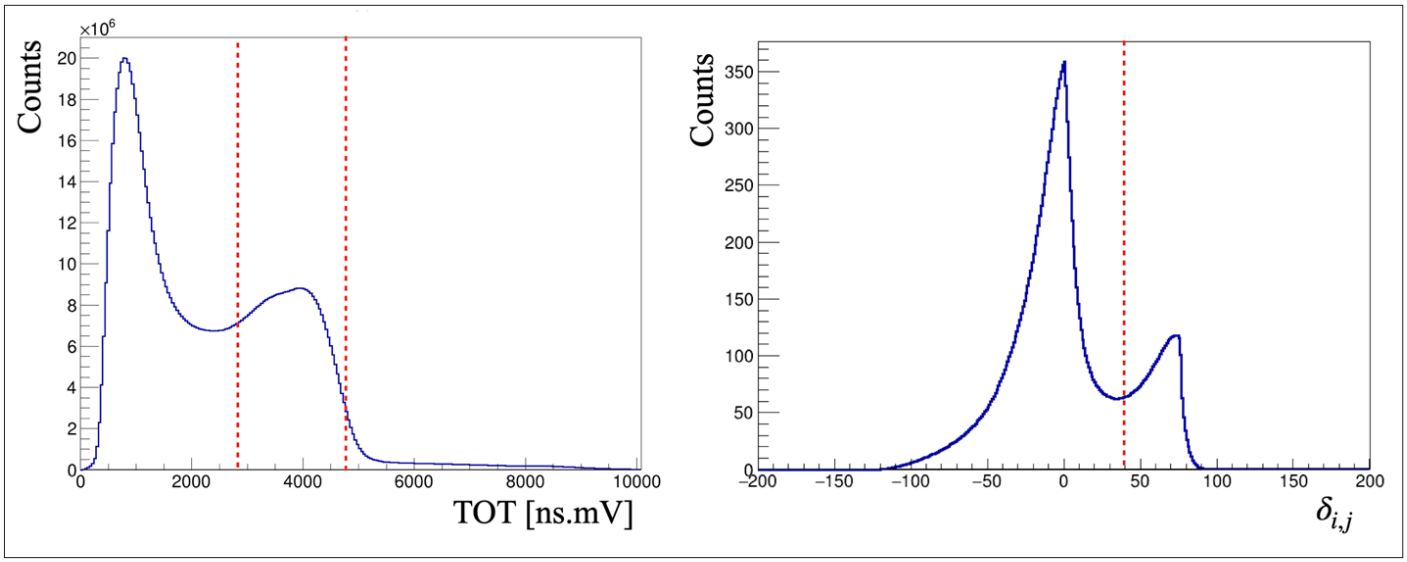

Fig. 3. (Left) Representative histogram showcasing the total time-over-threshold (TOT) for all scintillators, employed in photon identification. The TOT distribution corresponds to a 5 sleeves sensitivity phantom positioned at the center of the detector's FOV. Applied cuts are denoted by red dotted lines, (Right) Visualisation depicting the scatter test ($\delta_{i,j} = d_{i,j} - c \cdot |\Delta t_{i,j}|$) applied to all events involving a 5-sleeve sensitivity phantom located at the center of the detector's field of view. Secondary scattering interactions manifest with themselves small $\delta_{i,j}$ values and are therefore excluded from further analysis. Interactions exceeding a $\delta_{i,j}$ value of 40 cm are identified as primary photon candidates.

their recording times) as display in Fig. 3. Events with $\delta_{i,j} > 40$ cm were selected, reducing a substantial fraction of accidental coincidences spread across the entire ST range.

Monte Carlo modelling of the Modular J-PET

The Modular J-PET simulation has been carried out with the use of the Geant4 Application for Tomographic Emission (GATE) software (version 9.0) [32–36] based on the Geant4 toolkit (version 10-06) [37], which is used to simulate the interaction of these photons in the detector material. Simulations were performed using the list of physics processes emlivermore_polar. The model represents the interactions of photons and electrons with matter down to 10 eV and up to 100 GeV [38]. This range of energy suits well the region of interest in PET tomography. In simulation, just the material properties of the BC-404 scintillator (1.021.0606 g · cm^{-3}) [39] were simulated.

For the computation of the scanner's sensitivity, a simulation involving a 70 cm linear 2.6 MBq source of ^{68}Ge was conducted within the sensitivity phantom. This simulation was repeated while reducing the number of aluminium tubes from 5 to 1. Each simulation iteration involved positioning the source and phantom at two distinct locations: the central point of the FOV and an offset of 10 cm from the tomograph center, as depicted in Fig. 4. Simulations were performed, assuming the detection chamber, phantom, and source were placed in the air. To mitigate the influence of events involving photon scatter within the detector and phantom, simulated events underwent filtration based on specific criteria derived from correlations between the gamma quanta's time of interaction with the scintillator (hit time) and the

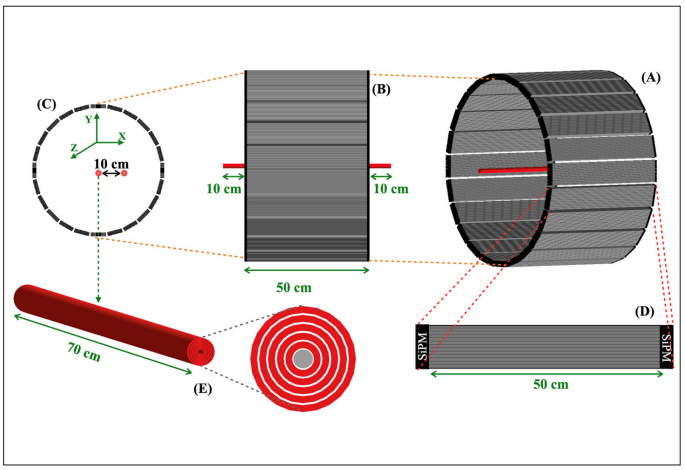

Fig. 4. (A) GATE visualisation of the Modular J-PET with sensitivity phantom located in the center of the FOV; (B) Side view of the Modular J-PET with the sensitivity phantom in the centre of the detectors FOV; (C) Cross section of Module J-PET, two red point present the position of sensitivity phantom inside the detector's FOV; (D) GATE visualisation of one module of Modular J-PET. The plastic scintillator strips are depicted in gray, while the SiPMs on both sides of the module are displayed in black; (E) GATE visualization of sensitivity Phantom with five sleeve tubes displayed with red and one polyethylene tube with length of 70 cm displayed with gray, also illustration of sensitivity phantom cross section. each sleeves has 2.5 mm thickness with different diameter according to NEMA--NU2_2018. The figure isn't to scale.

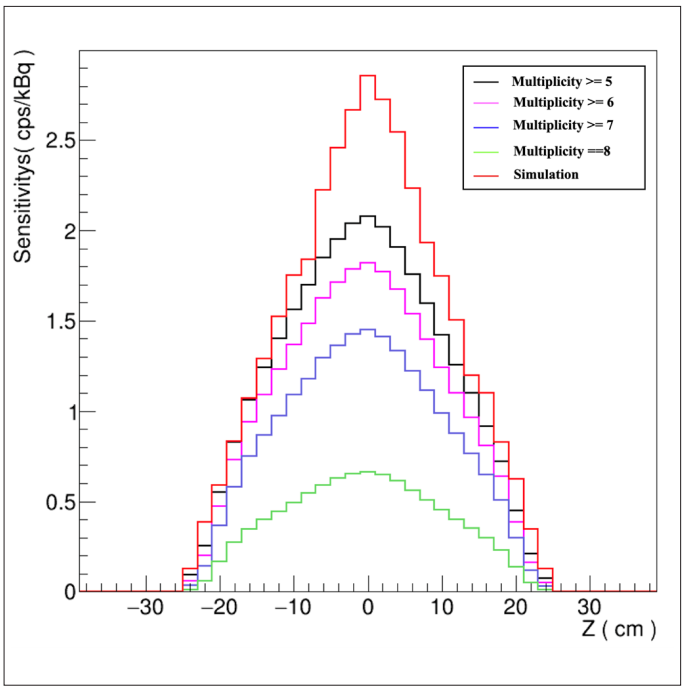

Fig. 5. Axial sensitivity profile for the smallest sleeve in the center of detector's FOV for experimental data and simulation data. Experimental data studied under different multiplicity cuts. The red line depicts the axial sensitivity profile at the center of the detector derived from simulation data. The peak point in the axial sensitivity profile defined as peak sensitivity and is equal to 2.9 cps/kBq for simulation data while the total system sensitivity is 1.32 ± 0.03 cps/kBq. In the experimental data for multiplicity cuts greater than or equal to 5, the peak sensitivity is 2.1 cps/kBq while the total system sensitivity is 1.03 ± 0.02 cps/kBq.

energy transferred by the gamma quanta to electrons within the material (energy deposition) [33].

Therefore, to extract true coincidences from the set of all coincidences, true coincidence events were defined, such as only events with two interactions registered with an energy loss larger than the fixed energy threshold of (200 keV). Moreover, it is required that Time of flight (TOF) is less than 3 ns. The study incorporated experimental resolutions in the dataset, encompassing a time resolution (FWHM) of 628 ps and an energy resolution of 0.23% at 340 keV. The dead time of 20 ns also applied to simulation. Furthermore, to suppress additional scattering coincidences during analysis, the scatter test cuts (ST > 40 cm) and geometry cut ($x^2 + y^2 \geq 30^2$, $|Z| \geq 25$cm) were applied to simulation data.

RESULTS

The determination of total sensitivity for both experimental and simulation data was accomplished using Equation 1 at specific positions. Tab. II. presents the total system sensitivities alongside their comparative analysis with simulation results.

Since the sensitivity is strongly dependent on the count rate after the application of all data selection criteria, altering the multiplicity criterion (Number of SiPMs connected to both ends of each detector module) distinctly affects both the axial sensitivity profile and the overall system sensitivity. The sensitivity of the Modular J-PET system across different multiplicity cuts (= 8, ≥7, ≥6, ≥5) at the center of detector's FOV was investigated. Fig. 5. illustrates the axial sensitivity profile for experimental data under various multiplicity cuts, with simulation results for a 1-sleeve phantom positioned at the center of detector's FOV. These simulated axial sensitivity profiles are in good agreement with experimental data employing a multiplicity cut of greater than or equal to 5. The peak sensitivity profile for experimental data with a multiplicity cut of ≥5 registered at 2.1 cps/kBq, while simulation results indicate 2.9 cps/kBq at the center of detector's FOV. These relatively minor differences were expected due to not modelled some electronic and digitizer parameters. Furthermore, the definition of detector--scattered coincidence events in the GATE software contributes to these differences.

DISCUSSION

The objectives of this work were to estimate and analyze the Sensitivity of the Modular J-PET system using the NEMA_NU2_2018 guidelines for system evaluation. NEMA norm requires estimations of sensitivity using 70 cm long linear source and the sensitivity phantom of the same length at two positions: centre of the detector`s FOV and 10 cm offset from the centre of the detectors FOV. To validate the experimental results, a Monte Carlo model of the Modular J-PET scanner was employed through the GATE simulation platform. The results obtained from simulations conducted on the 70 cm phantom

Tab. II. Comparison of the total system sensitivity and peak sensitivity profile for the simulation and experimental data at the center of detector's FOV and at 10 cm offset from the center of the detector's FOV.

	SOURCE AND PHANTOM POSITION	EXPERIMENTAL DATA		SIMULATION DATA
Total system sensitivity (cps/kBq)	In the centre of the detectors FOV	Multiplicity cuts ≥ 5	1.03 ± 0.002	1.32 ± 0.03
		Multiplicity cuts ≥ 6	0.95 ± 0.002	
		Multiplicity cuts ≥ 7	0.80 ± 0.001	
		Multiplicity cuts = 8	0.37 ± 0.001	
	In the 10 cm offset from the centre	Multiplicity cuts = 8	0.35 ± 0.003	1.31 ± 0.01
Peak sensitivity (cps/kBq)	In the centre of the detectors FOV	Multiplicity cuts ≥ 5	2.1	2.9
		Multiplicity cuts ≥ 6	1.9	
		Multiplicity cuts ≥ 7	1.5	
		Multiplicity cuts = 8	0.68	
	In the 10 cm offset from the centre	Multiplicity cuts = 8	0.62	2.8

exhibited concordance with the experimental measurements carried out on the Modular J-PET scanner.

The sensitivity of a PET scanner depends on the system's geometric acceptance, detection efficiency, and dead time. It means that the sensitivity depends on the scintillation decay time, density, atomic number, thickness of the detector material, the distance between the source and the detector, the diameter of the ring, and the number of detectors in the ring. For this reason, PET scanners made of LSO or BGO scintillators are more sensitive [40–43]. However, PET scans from plastic scintillators are economical. On the other hand, Large axial field of view scanner sensitivity increases significantly with axial length. The axial arrangement of detectors and utilized technology in the J-PET scanner leads to increased AFOV in the J-PET detector, just by extending the plastic scintillator length. Because the main geometrical difference between the J-PET tomograph and other PET scanners is the arrangement of scintillators and photodetectors. Also, increasing the distance between the detector and the source reduces the solid angle and thus decreases the geometric efficiency of the scanner and vice versa. Yet, the sensitivity of Modular J-PET may be further increased by adding a second detection layer or extending the AFOV [6]. The sensitivity of J-PET and crystal PET based scanners is evaluated and compared in the reference [40]. The aim of the study Modular J-PET scanner with a 50 cm long AFOV provided a an intermediate result for the development of cost-efficient Total--Body PET which is able to cover all of the patient's body [14].

CONCLUSIONS

The sensitivity profiles for the Modular J-PET scanner were assessed across various multiplicity cuts, revealing an increase in sensitivity as the multiplicity number decreases. This trend leads to comparable outcomes with simulations, notably for a multiplicity greater than or equal to 5. This congruence arises from the absence of optical photon simulations during the simulation phase. Specifically, the peak sensitivity profiles for experimental data, employing multiplicity cuts of greater than or equal to 5, and simulation data stand at 2.1 cps/kBq and 2.9 cps/kBq, respectively, at the detector's center. While the total system sensitivity in the centre of the detector`s FOV for experimental data, employing multiplicity cuts of greater than or equal to 5 is 1.03 ± 0.02 cps/kBq, and for simulation results, it is 1.32 ± 0.03 cps/kBq. Extending the length of the plastic scintillator strips and implementing a multi-layer PET scan are anticipated strategies to enhance the sensitivity of the Modular J-PET.

ACKNOWLEDGEMENTS

We acknowledge support from the Foundation for Polish Science through the TEAM POIR.04.04.00-00-4204/17 program, the National Science Centre of Poland through Grants No. 2021/42/A/ST2/00423, 2021/43/B/ST2/02150, 2019/35/B/ST2/03562, Jagiellonian University via Project No. CRP/0641.221.2020, and the SciMat and qLife Priority Research Area budget under the auspices of the program Excellence Initiative – Research University at Jagiellonian University.

REFERENCES

1. Alavi A, Werner T, Stepien E, Moskal P. Unparalleled and revolutionary impact of PET imaging on research and day to day practice of medicine. Bio-Algorithms and Med-Systems. 2021;17:203-12.
2. Vandenberghe S, Moskal P, Karp JS. State of the art in total body PET. EJNMMI Phys. 2020;7:35.
3. Surti S, Pantel AR, Karp JS. Total Body PET: Why, How, What for?. IEEE Trans Radiat Plasma Med Sci. 2020;4(3):283-92.
4. Alavi A, Saboury B, Nardo L, Zhang V, Wang M, Li H, et al. Potential and most relevant applications of total body PET/CT imaging. Clin Nucl Med. 2022;47:43-55.

5. Moskal P, Dulski K, Chug N, Curceanu C, Czerwiński E, Dadgar M, et al. Positronium imaging with the novel multi-photon PET scanner. Sci Adv. 2021;7:eabh4394.
6. Moskal P, Kowalski P, Shopa RY, Raczyński L, Baran J, Chug N, et al. Simulating NEMA characteristics of the modular total-body J-PET scanner—an economic total-body PET from plastic scintillators. Phys Med Biol. 2021;66:175015.
7. Moskal P, Niedźwiecki S, Bednarski T, Czerwiński E, Kapłon Ł, Kubicz E, et al. Test of a single module of the J-PET scanner based on plastic scintillators. Nucl Instrum Methods Phys Res A. 2014;764:317-28.
8. Moskal P, Zoń N, Bednarski T, Białas P, Czerwiński E, Gajos A, et al. A novel method for the line-of-response and time-of-flight reconstruction in TOF-PET detectors based on a library of synchronised model signals. Nucl Instrum Methods Phys Res A. 2015;775:54-80.
9. Niedźwiecki S, Białas P, Curceanu C, Czerwiński E, Dulski K, Gajos A. et al. J-PET: a new technology for the whole-body PET imaging. Acta Phys Polon B. 2017;48:1567-70.
10. Moskal P, Kisielewska D, Curceanu C, Czerwiński E, Dulski K, Gajos A, et al. Feasibility study of the positronium imaging with the J-PET tomograph. Phys Med Biol. 2019;64:055017.
11. Moskal P, Jasińska B, Stępień E, Bass SD. Positronium in Medicine and Biology. Nat. Rev. Phys. 2019;1(9):527-9.
12. Krzemien W, Alfs D, Białas P, Czerwiński E, Gajos A, et al. Overview of the software architecture and data flow for the J-PET tomography device. Acta Phys Polon B. 2016;47:561.
13. Kowalski P, Wiślicki W, Raczyński L, Alfs D, Bednarski T, Białas P, Głowacz B, et al. Scatter fraction of the J-PET tomography scanner. Acta Phys Polon B. 2016;47:549.
14. Moskal P, Stepien E. Prospects and clinical perspectives of total-body PET imaging using plastic scintillator. PET Clinics. 2020;15(4):439-52.
15. National Institute of Standards and Technology, 2020 [cited 2023 Dec 11]. Available from: https://nist.gov/pml.
16. Crystal [cited 2023 Dec 11]. Available from: https://www.crystals.saint-gobain.com/.
17. Vilardi I, Braem A, Chesi E, Ciocia F, Colonna N, Corsi F, et al. Optimization of the effective light attenuation length of YAP:Ce and LYSO:Ce crystals for a novel geometrical PET concept. Nucl Instrum Methods Phys Res. 2006;564:506-14.
18. Mao R, Zhang L, Zhu RY. Optical and Scintillation Properties of Inorganic Scintillators in High Energy Physics. IEEE Trans. Nucl. Sci. 2008;55:2425-31.
19. Korcyl G, Bialas P, Curceanu C, Czerwiński E, Dulski K, Flak B, et al. Evaluation of Single-Chip, Real-Time Tomographic Data Processing on FPGA SoC Devices. IEEE Trans. Med. Imaging. 2018;37(11).
20. Dadgar M, Parzych S, Tayefi Ardebili F. A Simulation Study to Estimate Optimum LOR Angular Acceptance for the Image Reconstruction with the Total-Body J-PET. Med Image Anal. 2021;12:189-200.
21. Dadgar M, Kowalski P. GATE Simulation Study of the 24-Module JPET Scanner: Data Analysis and Image Reconstruction. Acta Phys. Pol. B 2020;51:309-11.
22. Palka M, Strzempek P, Korcyl G, Bednarski T, Niedźwiecki S, Białas P, et al. Multichannel FPGA based MVT system for high precision time (20 ps RMS) and charge measurement. J. Instrum. 2017;12:08.
23. Kapłon L, Moskal G. Blue-emitting polystyrene scintillators for plastic scintillation dosimetry. Bio-Algorithms and Med-Systems. 2021;17(3):191-7.
24. Moskal P, Bednarski T, Niedzwiecki S, Silarski M, Czerwinski E, Kozik T, et al. Synchronization and Calibration of the 24-Modules J-PET Prototype With 300-mm Axial Field of View. IEEE Trans Instrum Meas. 2021;70:1-10.
25. NEMA Standards Publication NU 2-2018: Performance Measurements of Positron Emission Tomographs. National Electrical Manufacturers Association. Rosslyn VA, USA, 2018.
26. 3M [cited 2021 Mar 24]. Available from: https://www.3m.com.
27. Dupont [cited 2021 Mar 24]. Available from: https://www.dupont.com.
28. Kaplon L. Technical Attenuation Length Measurement of Plastic Scintillator Strips for the Total-Body J-PET Scanner. IEEE Trans. Nucl. Sci. 2020; 67(10): 2286-9.
29. Korcyl G, Białas P, Curceanu C, Czerwiński E, Dulski K, Flak B, et al. Evalation of single-chip, real-time tomographic data processing on fpga soc devices. IEEE Trans. Med. Imaging. 2018;37:2526-35.
30. Krzemien W, Gajos A, Kacprzak K, Rakoczy K, Korcyl G. J-pet framework: Software platform for pet tomography data reconstruction and analysis. SoftwareX. 2020;11:100487.
31. Sharma S, Chhokar J, Curceanu C, Czerwiński E, Dadgar M, Dulski K, et al. Estimating relationship between the Time Over Threshold and energy loss by photons in plastic scintillators used in the J-PET scanner. EJNMMI Phys. 2020;7:39.
32. Jan S, Santin G, Strul D, Staelens S, Assié K, Autret D, et al. GATE - Geant4 Application for Tomographic Emission: a simulation toolkit for PET and SPECT. Phys Med Biol. 2004; 49(19):4543–61.
33. Jan S, Benoit D, Becheva E, Carlier T, Cassol F, Descourt P, et al. GATE V6: a major enhancement of the GATE simulation platform enabling modelling of CT and radiotherapy. Phys Med Biol. 2011;56(4):881.
34. Sarrut D, Bała M, Bardies M, Bert J, Chauvin M, Chatzipapas K, et al. Advanced Monte Carlo simulations of emission tomography imaging systems with GATE. Phys Med Biol. 2021; 66(10):10TR03.
35. Agostinelli S, Allison J, Amako K, Apostolakis J, Araujo H, Arce P, et al. Geant4—a simulation toolkit. Nucl Instrum Methods Phys Res A: Accel Spectrom Detect Assoc Equip. 2003;506:250.
36. Kowalski P, Raczyński L, Bednarski T, Białas P, Czerwiński E, Giergiel K, et al. Determination of the map of efficiency of the Jagiellonian Positron Emission Tomograph (J-PET) detector with the GATE package. Bio-Algorithms and Med-Systems. 2014;10(2):85-90.
37. Allison J, Amako K, Apostolakis J, Arce P, Asai M, Aso T, et al. Recent developments in GEANT4. Nucl Instrum Methods Phys Res A: Accel Spectrom Detect Assoc Equip. 2016;835:186.
38. Kowalski P, Moskal P, Wislicki W, Raczynski L, Bednarski T, Bialas P, et al. Multiple scattering and accidental coincidences in the J-PET detector simulated using GATE package. Acta Phys Pol A. 2015;127:1505-12.
39. Eljentechnology [cited 2021 Mar 24]. Available from: https://eljentechnology.com/images/technical_library/Physical-Constants-Plastic.pdf.
40. Dadgar M, Parzych S, Baran J, Chug N, Curceanu C, Czerwiński E, et al. Comparative studies of the sensitivities of sparse and full geometries of Total-Body PET scanners built from crystals and plastic scintillators. EJNMMI Phys. 2023; 10(62).
41. Spencer B, Berg E, Schmall JP, Omidvari N, Leung EK, Abdelhafez YG, et al. Performance evaluation of the uExplorer total-body pet/ct scanner based on NEMA-nu 2-2018 with additional tests to characterize pet scanners with a long axial field of view. J Nucl Med. 2021;61:861.
42. Karp J, Viswanath V, Geagan MJ, Muehllehner G, Pantel AR, Parma MJ, et al. PennPET Explorer: Design and Preliminary Performance of a Whole-Body Imager. J Nucl Med. 2020;61(1):136-43.
43. Prenosil G, Sari H, Fürstner M, Afshar-Oromieh A, Shi K, Rominger A, et al. Performance Characteristics of the Biograph Vision Quadra PET/CT System with a Long Axial Field of View Using the NEMA NU 2-2018 Standard. J Nucl Med. 2022;63(3):476-84.